



# Vertical–horizontal coupling nonlinear vibration characteristics of rolling mill under mixed lubrication

Dong-xiao Hou<sup>1</sup> · Liang Xu<sup>1</sup> · Pei-ming Shi<sup>2</sup>

Received: 15 February 2020 / Revised: 17 July 2020 / Accepted: 20 July 2020 / Published online: 10 March 2021  
© China Iron and Steel Research Institute Group 2021

## Abstract

Considering the dynamic influence of the roll vibration on the lubricant film thickness in the rolling deformation area, nonlinear dynamic rolling forces related to film thickness in the vertical and horizontal directions were obtained based on the Karman's balance theory. Based on these dynamic rolling forces and the mechanical vibration of the rolling mill, a vertical–horizontal coupling nonlinear vibration dynamic model was established. The amplitude–frequency equation of the main resonance was derived by using the multiple-scale method. At last, the parameters of the 1780 rolling mill were used for numerical simulation, and the time-domain response curves of the system's vibration displacement and lubricating film thickness under the steady and unsteady conditions were analyzed. The influences of parameters such as interface contact ratio, nonlinear parameters and external disturbances on the primary resonance frequency characteristics were obtained, which provided a theoretical reference for the suppression of rolling mill vibration.

**Keywords** Vertical–horizontal coupling · Nonlinear vibration · Mixed lubrication · Dynamic rolling force · Main resonance · Amplitude–frequency characteristic

## List of symbols

$A$  Function related to time scale in horizontal solution  
 $\bar{A}$  Conjugation of  $A$   
 $B$  Function related to time scale in vertical solution  
 $\bar{B}$  Conjugation of  $B$   
 $a$  Vibration amplitude in horizontal direction  
 $b$  Vibration amplitude in vertical direction  
 $c_1$  Equivalent damping in horizontal direction  
 $c_2$  Equivalent damping in vertical direction  
 $cc$  Conjugation of the previous items  
 $F_1$  External disturbance force amplitude in horizontal direction

$F_2$  External disturbance force amplitude in the vertical direction  
 $F_x$  Dynamic rolling force in horizontal direction  
 $F_y$  Dynamic rolling force in vertical direction  
 $F'_x$  Steady part of dynamic rolling force in horizontal direction  
 $F'_y$  Steady part of dynamic rolling force in vertical direction  
 $k_1$  Equivalent stiffness in horizontal direction  
 $k_2$  Equivalent stiffness in vertical direction  
 $l$  Deformation area length  
 $m_1$  Equivalent mass of work roll  
 $o_1$  Center of upper work roll  
 $o_2$  Center of lower work roll  
 $p$  Rolling pressure in deformation area  
 $p_a$  Pressure from dry friction  
 $p_b$  Pressure from fluid lubrication friction  
 $P_1$  External disturbance in horizontal direction  
 $P_2$  External disturbance in vertical direction  
 $R$  Roll radius  
 $s$  Back tension of strip  
 $t$  Time  
 $T_n$  Different time scales  
 $u_e$  Entrance speed of strip  
 $u(x)$  Speed of strip in deformation area

✉ Liang Xu  
xl13081858287@163.com  
Dong-xiao Hou  
houdongxiao1982@163.com  
Pei-ming Shi  
spmysu@qq.com

<sup>1</sup> School of Control Engineering, Northeastern University at Qinhuangdao, Qinhuangdao 066004, Hebei, China

<sup>2</sup> School of Electrical Engineering, Yanshan University, Qinhuangdao 066004, Hebei, China

$\bar{u}$	Average speed of roller and strip
$v_R$	Roll speed
$v'_R$	Roll speed during vibration
$x_0$	Amplitude under $T_0$ time scale in horizontal direction
$x_1$	Amplitude under $T_1$ time scale in horizontal direction
$x_c$	Roll vibration displacement in horizontal direction
$x_{c0}$	Horizontal displacement of roll during steady rolling
$x_d$	Exit position during vibration
$x_e$	Deformation zone length during vibration
$x_n$	Neutral position
$X$	Dimensionless deformation area
$y_0$	Amplitude under $T_0$ time scale in vertical direction
$y_1$	Amplitude under $T_1$ time scale in vertical direction
$y_e$	Entrance thickness of strip
$y_d$	Exit thickness of strip
$y'_d$	Roll gap height
$y_c$	Roll vibration displacement in vertical direction
$y_{c0}$	Vertical displacement of roll during steady rolling
$y(x)$	Strip thickness in deformation area
$z$	Lubricating film thickness in deformation area
$z_0$	Film thickness under $T_0$ time scale
$z_1$	Film thickness under $T_1$ time scale
$z_c$	Lubricant film thickness at junction of entrance area and deformation area
$z_q$	Lubricant film thickness at entrance area
$\gamma$	Emulsion viscosity–pressure coefficient
$\varepsilon$	Small parameters
$\theta$	Entrance angle
$\lambda$	Contact ratio between interfaces
$\mu$	Emulsion viscosity
$\mu_0$	Emulsion viscosity at standard atmospheric pressure
$\sigma$	Yield strength of strip
$\sigma_1$	Horizontal coordination factor
$\sigma_2$	Vertical coordination factor
$\tau_a$	Shear stress caused by dry friction
$\tau_b$	Shear stress caused by fluid friction
$\tau_s$	Shear stress on strip
$\varphi_1$	Angle parameter when solving $A$
$\varphi_2$	Angle parameter when solving $B$
$\omega_1$	Undamped natural frequency in horizontal direction
$\omega_2$	Undamped natural frequency in vertical direction
$\Delta F_x$	Dynamic part of dynamic rolling force in horizontal direction
$\Delta F_y$	Dynamic part of dynamic rolling force in vertical direction
$\Omega_1$	External disturbance frequency in horizontal direction
$\Omega_2$	External disturbance frequency in vertical direction

## 1 Introduction

The vibration phenomenon of the rolling mill always exists during working. The vibration of the rolling mill not only reduces the quality of the products, but also damages the equipment in severe cases and even leads to huge economic losses [1, 2]. In order to avoid the vibration of the rolling mill, a lot of research work has been carried out in recent years [3–7]. Based on the rolling force model of Sims, Wang and Yan established a dynamic vertical vibration model considering entrance thickness deviation [8]. Liu et al. [9] established a hysteresis nonlinear vertical vibration model of the rolling mill considering the hysteresis nonlinear effect of roll elastoplastic deformation, and the stability of the hysteresis nonlinear system was analyzed by using the singularity stability theory. Liu et al. [10] established a torsional–horizontal coupling vibration model, in which the static bifurcation characteristics were studied by using the singularity theory, and the branching conditions and stability were studied by using the Hopf bifurcation theorem. The coupled vibration of the rolling mill among the vertical, horizontal and torsional directions is also one of the research hotspots. Lu et al. [11] studied the effect of various rolling conditions on the stability of the continuous rolling mill. Zeng et al. [12] analyzed the stability of the system with different process parameters and structural parameters.

The friction between the strip and the roll in the deformation area has a great influence on the vibration of the rolling mill. Li et al. [13] proposed a friction coefficient model for rolling force calculation, and a new solution method for rolling force calculation formula was established, with its accuracy higher than that of the traditional Sims model. Hou et al. [14] studied the vertical–horizontal coupled vibration characteristics by considering the friction as the dry friction model. A nonlinear friction model was used in vertical–torsional–horizontal coupling dynamic model by Zeng et al. [15], and the stability region was analyzed by using the Hopf bifurcation algebra criterion. Liu et al. [16] used the regression index function model of friction coefficient in the dynamic rolling process model, and a vibration model with unsteady lubrication was established. Wang et al. [17] established a multi-coupling model of interface membrane constraints and quantitatively analyzed the effects of some main parameters on the critical velocity and amplitude of vertical vibration.

In this paper, the mixed lubrication friction model was used to replace the dry friction model in the Karman differential equation, and the film thickness calculated by the average flow Reynolds formula was brought into the calculation to obtain a new dynamic rolling force expression. Considering the impact of roll vibration displacement and

film thickness on dynamic rolling force, a vertical–horizontal coupled vibration model was established and solved by using the multi-scale method. Finally, the actual rolling mill parameters were used for numerical simulation and related dynamic analysis.

## 2 Rolling mill system modeling

### 2.1 Unsteady lubrication model under roll vibration

Considering the influence of lubrication friction, the strip interface is divided into an entrance area, a deformation area and an exit area. The schematic diagram is shown in Fig. 1. The pressure reaches a maximum at the junction of the entrance area and the deformation area due to wedge effect.

The expression of the emulsion pressure distribution in the entrance area can be determined by the average flow Reynolds equation as follows [18].

$$\frac{\partial}{\partial x} \left( \frac{z_q^3}{12\mu} \frac{\partial p}{\partial x} \right) = -\frac{u_e + v_R}{2} \frac{\partial z_q}{\partial x} + \frac{\partial z_q}{\partial t} \tag{1}$$

When the roll vibrates, the horizontal speed component of the roll can be expressed as

$$v'_R = v_R + \dot{x}_c \tag{2}$$

It is assumed that  $z_q$  can be written as a function of position  $x$  in the entrance region.

$$z_q = z_c + \theta(x - x_e) \tag{3}$$

Integrating Eq. (1), the pressure gradient can be obtained as

$$\frac{z_q^3}{12\mu} \frac{\partial p}{\partial x} = (\dot{z}_q - \theta\bar{u})(x - x_e) + \frac{1}{2}\dot{\theta}(x - x_e)^2 + f(t) \tag{4}$$

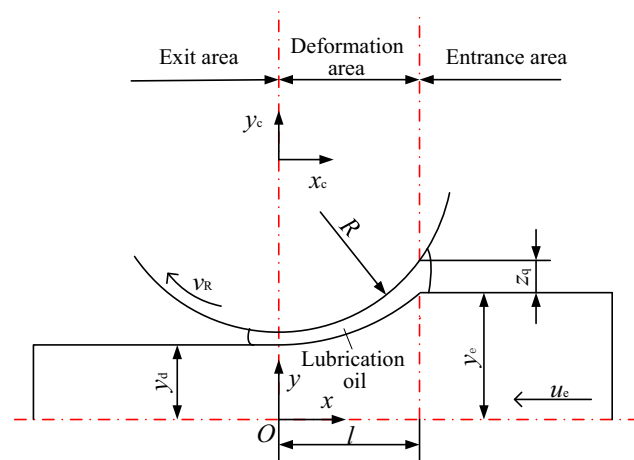


Fig. 1 Lubrication friction schematic of rolling interface

where  $\bar{u} = \frac{u_e + v_R + \dot{x}_c}{2}$ ; and  $f(t)$  is an arbitrary time function.

Ignoring pressure gradients in the entrance area, that is  $\frac{\partial p}{\partial x} = 0$ ,  $f(t) = 0$  can be obtained.

As a result of large pressure at the entrance area, it is assumed that  $\mu$  changes with the pressure. The Barus viscosity formula [19] can be used as follows

$$\mu = \mu_0 e^{\gamma p} \tag{5}$$

In order to simplify the analysis, supposing  $\phi = e^{-\gamma p}$ , according to Eq. (5), the deformation of  $\phi$  can be written as

$$\phi = 1 + \frac{12\gamma\mu_0}{\theta} \left( \bar{u} - \frac{\dot{z}_c}{\theta} \right) \left( -\frac{1}{z_q} + \frac{z_c}{2z_q^2} \right) - 6\gamma\mu_0\dot{\theta}C_R \tag{6}$$

where  $C_R = \frac{R^2\theta C_1}{z_c C_2} + \frac{R^2\theta C_1}{C_2\sqrt{a}C_2} \ln \left( \frac{R\theta - \sqrt{RC_2}}{R\theta + \sqrt{RC_2}} \right)$ ;  $C_1 = 2R\theta^2 - z_c$ ; and  $C_2 = R\theta^2 - 2z_c$ .

The boundary conditions at the edge of the entrance area are  $x = 0$  and  $z = z_c$ , and the Tresca yield criterion is used to calculate  $p$ .

$$p = \sigma - s \tag{7}$$

Substituting Eq. (7) into Eq. (6), the following equation can be obtained

$$1 - e^{-\gamma(\sigma-s)} = 6\gamma\mu_0\dot{\theta}C_R + \frac{6\gamma\mu_0}{z_c\theta} \left( \bar{u} - \frac{\dot{z}_c}{\theta} \right) \tag{8}$$

The change rate of the entrance film thickness can be calculated from Eq. (8)

$$\dot{z}_c = \theta\bar{u} + \theta^2 z_c \dot{\theta} C_R - \frac{1 - e^{-\gamma(\sigma-s)}}{6\gamma\mu_0} \theta^2 z_c \tag{9}$$

The change rate of the entrance angle is ignored because the change is small, that is  $\dot{\theta} = 0$ , and then, the differential equation of the film thickness in the case of vibration is obtained.

$$\dot{z}_c = \theta\bar{u} - \frac{1 - e^{-\gamma(\sigma-s)}}{6\gamma\mu_0} \theta^2 z_c \tag{10}$$

## 2.2 Nonlinear dynamic rolling force model

### 2.2.1 Parameters of deformation zone when roll vibrates

Figure 2 shows the diagram of a rolling process model. Considering that the shape of the strip in the deformation area is similar to a parabola [20], the strip thickness  $y(x)$  at any position  $x$  in the deformation area can be expressed as

$$y(x) = y_d + 2y_c + \frac{(x - x_c)^2}{R} \tag{11}$$

The distance from the centers of two rolls to the entrance of the deformation area can be obtained from Eq. (11).

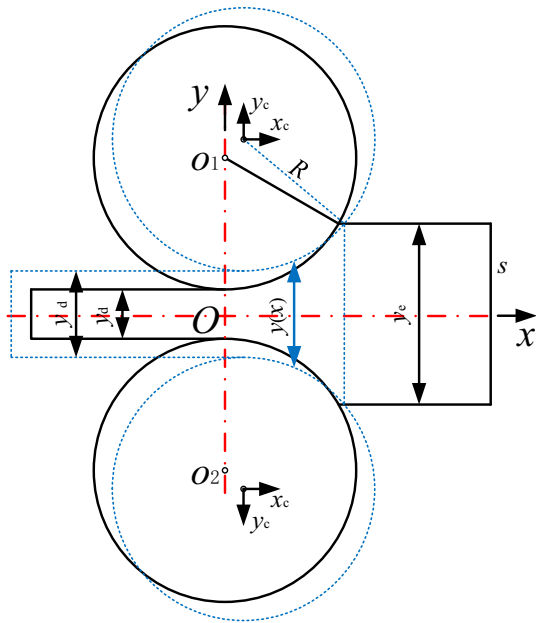


Fig. 2 Model of rolling process

$$x_e = x_c + \sqrt{R(y_e - y_d - 2y_c)} \tag{12}$$

The rolling speed of the strip at the neutral point can be obtained according to the metal second flow correction equation (Eq. (13)) proposed by Hu and Ehmann [21] and it is equal to the roll speed.

$$u(x)y(x) = u_e y_e - 2(x_e - x)y'_c + (y_e - y(x))\dot{x}_c \tag{13}$$

$$u(x) = \frac{u_e y_e - 2(x_e - x_n)y'_c + (y_e - y(x))\dot{x}_c}{y(x)} = v_R \tag{14}$$

The neutral point coordinates can be obtained from Eq. (14).

$$x_n = x_c + \frac{\dot{y}_c R}{v_R + \dot{x}_c} + \sqrt{\frac{CR}{v_R + \dot{x}_c} + \left(\frac{\dot{y}_c R}{v_R + \dot{x}_c}\right)^2} \tag{15}$$

where

$$C = u_e y_e - 2(x_e - x_c)y'_c + (y_e - y'_d)\dot{x}_c - v_R y'_d$$

$$\text{and } y'_d = y_d + 2y_c.$$

### 2.2.2 Determination of nonlinear dynamic rolling force

According to the slab analysis method, an arbitrary microelement in the deformation area is shown in Fig. 3. According to the Karman's theory of force balance, a differential equation of  $p$  and  $y(x)$  can be obtained

$$(p + \sigma) \frac{dy(x)}{dx} + y(x) \frac{d\sigma}{dx} \mp 2\tau_s = 0 \tag{16}$$

when  $x < x_n$ , take the negative and when  $x_n < x$ , take the positive.

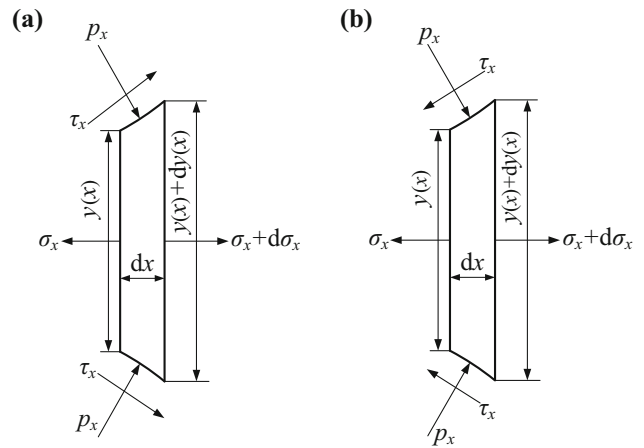


Fig. 3 Stress diagram of strip. **a** Forward slide zone; **b** backward slide zone.  $\sigma_x$  Normal stress

Substituting Eq. (7) into Eq. (16) and simplifying it, the following equations could be obtained

$$\sigma \frac{dy(x)}{dx} - y(x) \frac{dp}{dx} \mp 2\tau_s = 0 \tag{17}$$

$$\tau_s = \lambda \tau_a + (1 - \lambda) \tau_b \tag{18}$$

$\tau_a$  of the rough contact surface boundary can be calculated by adhesive friction theory.

$$\tau_a = \frac{\sigma}{2} \tag{19}$$

$\tau_b$  can be calculated according to Eq. (20).

$$\tau_b = \mu_0 \frac{u(x) - v_R}{z} \tag{20}$$

Substituting Eqs. (19) and (20) into Eq. (17) and arranging them, following equation can be obtained:

$$\lambda \left( \sigma \frac{dy(x)}{dx} - y(x) \frac{dp_a}{dx} \mp \sigma \right) + (1 - \lambda) \left( \sigma \frac{dy(x)}{dx} - y(x) \frac{dp_b}{dx} \mp 2\mu_0 \frac{u(x) - v_R}{z} \right) = 0 \tag{21}$$

Since both  $p_a$  and  $p_b$  are greater than zero under the mixed lubrication friction state, both parts must be equal to zero at the same time if the equation is true.

$$\begin{cases} \sigma \frac{dy(x)}{dx} - y(x) \frac{dp_a}{dx} \mp \sigma = 0 \\ \sigma \frac{dy(x)}{dx} - y(x) \frac{dp_b}{dx} \mp 2\mu_0 \frac{u(x) - v_R}{z} = 0 \\ p(x) = \lambda p_a + (1 - \lambda) p_b \end{cases} \tag{22}$$

where  $p(x)$  is a function of  $p$  with respect to  $x$ .

Then, the rolling force in the vertical and horizontal directions can be calculated by Eq. (23).

$$\begin{cases} F_x = \int_{x_d}^{x_e} p(x) \tan \theta dx \mp \int_{x_d}^{x_e} \tau_s dx \\ F_y = \int_{x_d}^{x_e} p(x) dx \mp \int_{x_d}^{x_e} \tau_s \tan \theta dx \end{cases} \quad (23)$$

where  $\tan \theta = \frac{x-x_c}{\sqrt{R^2-(x-x_c)^2}}$ ; because  $(x-x_c) \ll R$ ,  $\tan \theta = \frac{x-x_c}{R}$ .

$F_x$  and  $F_y$  in the vertical and horizontal directions can be written as

$$\begin{aligned} F_x = & \lambda \sigma \left[ -2x_n \sqrt{\frac{R}{y'_d}} \tan^{-1} \left( \frac{x_n}{\sqrt{Ry'_d}} \right) - R \ln \left( \frac{x_n^2 + Ry'_d}{Ry'_d} \right) + \right. \\ & R \sqrt{\frac{y_e - y'_d}{y'_d}} \tan^{-1} \left( \sqrt{\frac{y_e - y'_d}{y'_d}} \right) - \frac{R}{2} \ln \left( \frac{y_e}{y'_d} \right) \left. \right] + \\ & \frac{2E(1-\lambda)}{R} \left[ \frac{u_e^2 y_e^2 R^3}{2(Ry'_d + x_n^2)} - \frac{u_e^2 y_e^2 R^2}{4y'_d} - \frac{u_e^2 y_e^2 R^2}{4} + \right. \\ & \left. \frac{2v_R^2}{\sqrt{Ry'_d}} \left( \tan^{-1} \left( \frac{x_n}{\sqrt{Ry'_d}} \right) - \tan^{-1} \left( \sqrt{\frac{y_e - y'_d}{y'_d}} \right) \right) \right] + \\ & \frac{\lambda \sigma}{2} (x_e - 2x_n) + E(1-\lambda)v_R^2(2x_n - x_e) + u_e^2 y_e^2 E(1-\lambda) \\ & \left[ \int_{x_n}^{x_e} \frac{R^2}{(Ry'_d - x^2)^2} dx - \int_{x_d}^{x_n} \frac{R^2}{(Ry'_d - x^2)^2} dx \right] \end{aligned} \quad (24)$$

$$\begin{aligned} F_y = & \lambda \sigma \left[ -2x_n \sqrt{\frac{R}{y'_d}} \tan^{-1} \left( \frac{x_n}{\sqrt{Ry'_d}} \right) + R \ln \left( \frac{x_n^2 + Ry'_d}{Ry'_d} \right) + \right. \\ & R \sqrt{\frac{y_e - y'_d}{y'_d}} \tan^{-1} \left( \sqrt{\frac{y_e - y'_d}{y'_d}} \right) - \frac{R}{2} \ln \left( \frac{y_e}{y'_d} \right) \left. \right] + \\ & \sigma \left[ x_e \ln \left( \frac{y_e}{y'_d} \right) - 2x_e + 2\sqrt{Ry'_d} \tan^{-1} \left( \sqrt{\frac{y_e - y'_d}{y'_d}} \right) \right] + \\ & (1-\lambda)\sigma \left[ -2x_e + 2\sqrt{Ry'_d} \tan^{-1} \left( \sqrt{\frac{y_e - y'_d}{y'_d}} \right) \right] + \\ & (1-\lambda)Ev_R^2 \sqrt{\frac{R}{y'_d}} \left[ 2x_n \sqrt{\frac{R}{y'_d}} \tan^{-1} \left( \frac{x_n}{\sqrt{Ry'_d}} \right) - \right. \\ & x_e \tan^{-1} \left( \sqrt{\frac{y_e - y'_d}{y'_d}} \right) - \sqrt{Ry'_d} \ln \left( \frac{x_n^2 + Ry'_d}{Ry'_d} \right) + \\ & \left. \frac{\sqrt{Ry'_d}}{2} \ln \left( \frac{y_e}{y'_d} \right) \right] + (1-\lambda)Eu_e^2 y_e^2 \int_{x_d}^{x_e} \int_{x_d}^x \mp \frac{1}{y(x)^3} dx dx + \\ & \frac{\lambda \sigma}{2R} (x_e^2 - x_n^2) + \frac{E(1-\lambda)}{R} \left[ v_R^2 (x_n^2 - \frac{x_e^2}{2}) \right] + \\ & \frac{u_e^2 y_e^2 R^2}{2} \left( \frac{2}{Ry'_d + x_n^2} - \frac{1}{Ry_e} - \frac{1}{Ry'_d} \right) \end{aligned} \quad (25)$$

where  $E = \frac{2\mu_0 z_c}{u_e + v_R}$ ,  $x_d = x_c$ ; when  $x_d < x < x_n$ , take the negative and when  $x_n < x < x_e$ , take the positive.

### 2.3 Vertical–horizontal coupling vibration model of rolling mill

Supposing that the point  $(x_{c0}, y_{c0})$  is the equilibrium point when the roll vibrates, the steady vibration speeds of roll are  $\dot{x}_c = 0$  and  $\dot{y}_c = 0$ .  $F_x$  and  $F_y$  are Taylor-expanded at the equilibrium point  $(x_{c0}, y_{c0}, 0, 0, z_c)$ .

$$\begin{cases} F_x = F'_x + \Delta F_x \\ F_y = F'_y + \Delta F_y \end{cases} \quad (26)$$

Taking the first and third terms of Taylor expansion of  $\Delta F_x$  and  $\Delta F_y$ , the followings could be obtained

$$\begin{cases} \Delta F_x(x_c, y_c, \dot{x}_c, \dot{y}_c, z_c) = a_1 x_c + a_2 y_c + a_3 \dot{x}_c + a_4 \dot{y}_c + \\ \quad a_5 z_c + a_6 x_c^3 + a_7 y_c^3 \\ \Delta F_y(x_c, y_c, \dot{x}_c, \dot{y}_c, z_c) = b_1 x_c + b_2 y_c + b_3 \dot{x}_c + b_4 \dot{y}_c + \\ \quad b_5 z_c + b_6 x_c^3 + b_7 y_c^3 \end{cases} \quad (27)$$

Since the structure of the rolling mill is symmetrical, the four-degrees-of-freedom dynamic equation is reduced to two-degrees-of-freedom.

$$\begin{cases} m_1 \ddot{x}_c + c_1 \dot{x}_c + k_1(x_c + x_{c0}) + F_x = P_1 \\ m_1 \ddot{y}_c + c_2 \dot{y}_c + k_2(y_c + y_{c0}) + F_y = P_2 \end{cases} \quad (28)$$

There are  $\ddot{x}_c = \ddot{y}_c = 0$ ,  $\dot{x}_c = \dot{y}_c = 0$ ,  $x_c = y_c = 0$ , and  $z_c = z_{c0}$  in steady state. After these conditions are brought into Eq. (28), the following equations can be obtained

$$\begin{cases} k_1 x_{c0} + F_x(x_{c0}, 2y_{c0}, 0, 0, 2z_c) = 0 \\ k_2 y_{c0} + F_y(x_{c0}, 2y_{c0}, 0, 0, 2z_c) = 0 \end{cases} \quad (29)$$

Substituting Eq. (29) into Eq. (28) and eliminating stable term, the equations can be simplified as

$$\begin{cases} m_1 \ddot{x}_c + c_1 \dot{x}_c + k_1 x_c + \Delta F_x = P_1 \\ m_1 \ddot{y}_c + c_2 \dot{y}_c + k_2 y_c + \Delta F_y = P_2 \end{cases} \quad (30)$$

Substituting Eq. (27) into Eq. (30), and dimensionless coefficients of the equations,  $\alpha_1 = \frac{c_1 + a_3}{m_1}$ ,  $\alpha_2 = \frac{c_2 + b_4}{m_1}$ ,  $\omega_1^2 = \frac{k_1 + a_1}{m_1}$ ,  $\omega_2^2 = \frac{k_2 + b_2}{m_1}$ ,  $\beta_1 = \frac{a_2}{m_1}$ ,  $\beta_2 = \frac{b_1}{m_1}$ ,  $\rho_1 = \frac{a_4}{m_1}$ ,  $\rho_2 = \frac{b_3}{m_1}$ ,  $\varsigma_1 = \frac{a_5}{m_1}$ ,  $\varsigma_2 = \frac{b_5}{m_1}$ ,  $\zeta_1 = \frac{a_6}{m_1}$ ,  $\zeta_2 = \frac{b_6}{m_1}$ ,  $\eta_1 = \frac{a_7}{m_1}$ ,  $\eta_2 = \frac{b_7}{m_1}$ ,  $\Delta P_1 = \frac{P_1}{m_1}$ ,  $\Delta P_2 = \frac{P_2}{m_1}$ , and combining these dimensionless equations with Eq. (10), the differential equations related to film thickness can be obtained as follows:

$$\begin{cases} \ddot{x}_c + \alpha_1 \dot{x}_c + \omega_1^2 x_c + \beta_1 y_c + \rho_1 \dot{y}_c + \varsigma_1 z_c + \xi_1 x_c^3 + \eta_1 y_c^3 = \Delta P_1 \\ \ddot{y}_c + \alpha_2 \dot{y}_c + \omega_2^2 y_c + \beta_2 x_c + \rho_2 \dot{x}_c + \varsigma_2 z_c + \xi_2 x_c^3 + \eta_2 y_c^3 = \Delta P_2 \\ \dot{z}_c + \varphi z_c = \theta \bar{u} + \frac{\theta}{2} \dot{x}_c \end{cases} \tag{31}$$

where  $\varphi = \frac{\theta^2(1-e^{-\gamma(\sigma-s)})}{6\gamma\mu_0}$ .

### 3 Model solving

#### 3.1 Solving coupled vibration models

The external disturbance of the rolling mill is set as  $\Delta P_1 = F_1 \cos(\Omega_1 t)$  and  $\Delta P_2 = F_2 \cos(\Omega_2 t)$ . Assuming that the vertical–horizontal coupled vibration system is a weak nonlinear system, the nonlinear terms are taken as a small parameter  $\varepsilon$ , and then Eq. (31) can be written as the following equations.

$$\begin{cases} \ddot{x}_c + \omega_1^2 x_c = -\varepsilon[\alpha_1 \dot{x}_c + \rho_1 \dot{y}_c + \beta_1 y_c + \varsigma_1 z_c + \xi_1 x_c^3 + \eta_1 y_c^3 - F_1 \cos(\Omega_1 t)] \\ \ddot{y}_c + \omega_2^2 y_c = -\varepsilon[\alpha_2 \dot{y}_c + \rho_2 \dot{x}_c + \beta_2 x_c + \varsigma_2 z_c + \xi_2 x_c^3 + \eta_2 y_c^3 - F_2 \cos(\Omega_2 t)] \\ \dot{z}_c = -\varepsilon\left(-\frac{\theta}{2} x_c + \dot{z}_c + \theta \bar{u}\right) \end{cases} \tag{32}$$

Substituting Eq. (34) into Eq. (32), taking the term with the same power exponent on both sides of the equal sign, and sorting them out, the following equations are obtained.

$$\begin{cases} D_0^2 x_0 + \omega_1^2 x_0 = 0 \\ D_0^2 y_0 + \omega_2^2 y_0 = 0 \\ \varphi z_0 = 0 \end{cases} \tag{35}$$

$$\begin{cases} D_0^2 x_1 + \omega_1^2 x_1 = -2D_0 D_1 x_0 - \alpha_1 D_0 x_0 - \rho_1 D_0 y_0 - \beta_1 y_0 - \varsigma_1 z_0 - \xi_1 x_0^3 - \eta_1 y_0^3 + F_1 \cos(\Omega_1 t) \\ D_0^2 y_1 + \omega_2^2 y_1 = -2D_0 D_1 y_0 - \alpha_2 D_0 y_0 - \rho_2 D_0 x_0 - \beta_2 x_0 - \varsigma_2 z_0 - \xi_2 x_0^3 - \eta_2 y_0^3 + F_2 \cos(\Omega_2 t) \\ \varphi z_1 = -\frac{\theta}{2} D_0 x_0 + D_0 z_0 + \theta \bar{u} \end{cases} \tag{36}$$

It can be seen that  $z_0 = 0$ . The solution of Eq. (35) is set as the following equation

$$\begin{cases} x_0 = A(T_1) \exp(i\omega_1 T_0) + \bar{A} \exp(-i\omega_1 T_0) \\ y_0 = B(T_1) \exp(i\omega_2 T_0) + \bar{B} \exp(-i\omega_2 T_0) \end{cases} \tag{37}$$

Substituting Eq. (37) into Eq. (36), then, Eq. (36) can be rewritten as

$$\begin{cases} D_0^2 x_1 + \omega_1^2 x_1 = \frac{1}{2} F_1 \exp(i\Omega_1 T_0) + (-2i\omega_1 D_1 A - i\omega_1 \alpha_1 A - 3\xi_1 A^2 \bar{A}) \exp(i\omega_1 T_0) \\ \quad - (\beta_1 B + i\omega_2 \rho_1 B + 3\eta_1 B^2 \bar{B}) \exp(i\omega_2 T_0) - \xi_1 A^3 \exp(3i\omega_1 T_0) - \eta_1 B^3 \exp(3i\omega_2 T_0) + cc \\ D_0^2 y_1 + \omega_2^2 y_1 = \frac{1}{2} F_2 \exp(i\Omega_2 T_0) + (-2i\omega_2 D_1 B - i\omega_2 \alpha_2 B - 3\eta_2 B^2 \bar{B}) \exp(i\omega_2 T_0) \\ \quad - (\beta_2 A + i\omega_1 \rho_2 A + 3\xi_1 A^2 \bar{A}) \exp(i\omega_1 T_0) - \xi_2 A^3 \exp(3i\omega_1 T_0) - \eta_2 B^3 \exp(3i\omega_2 T_0) + cc \\ z_1 = \frac{1}{\varphi} \left( -\frac{\theta}{2} D_0 x_0 + D_0 z_0 + \theta \bar{u} \right) \end{cases} \tag{38}$$

Multiple-scale method is a method of introducing different time scales.

$$\begin{cases} T_n = \varepsilon^n t, \quad n = 0, 1, 2, \dots \\ \frac{d}{dt} = D_0 + \varepsilon D_1 \\ \frac{d^2}{dt^2} = D_0^2 + 2\varepsilon D_0 D_1 + \varepsilon^2 (D_1^2 + 2D_0 D_2) + \dots \end{cases} \tag{33}$$

where  $D_n$  is  $\frac{\partial}{\partial T_n}$ ,  $n = 0, 1$ ;

The solution of Eq. (31) can be set as

$$\begin{cases} x_c = x_0(T_0, T_1) + \varepsilon x_1(T_0, T_1) + \dots \\ y_c = y_0(T_0, T_1) + \varepsilon y_1(T_0, T_1) + \dots \\ z_c = z_0(T_0, T_1) + \varepsilon z_1(T_0, T_1) + \dots \end{cases} \tag{34}$$

#### 3.2 Main resonance solution

Assuming that  $\Omega_1 = \omega_1 + \varepsilon\sigma_1$ ,  $\Omega_2 = \omega_2 + \varepsilon\sigma_2$ , the following equations can be obtained by eliminating the long-term terms

$$\begin{cases} -2i\omega_1 D_1 A - i\omega_1 \alpha_1 A - 3\xi_1 A^2 \bar{A} + \frac{1}{2} F_1 \exp(i\sigma_1 T_1) = 0 \\ -2i\omega_2 D_1 B - i\omega_2 \alpha_2 B - 3\eta_2 B^2 \bar{B} + \frac{1}{2} F_2 \exp(i\sigma_2 T_1) = 0 \end{cases} \tag{39}$$

Amplitudes  $A$  and  $B$  in Eq. (37) are expressed in polar coordinates.



$$\begin{cases} A = \frac{1}{2} a(T_1) \exp[i\varphi_1(T_1)] \\ B = \frac{1}{2} b(T_1) \exp[i\varphi_2(T_1)] \end{cases} \quad (40)$$

Substituting Eq. (40) into Eq. (39), separating the imaginary and real parts, and setting  $\psi_1 = \sigma_1 T_1 - \varphi_1$ ,  $\psi_2 = \sigma_2 T_1 - \varphi_2$ , it can be obtained that

$$\begin{cases} \dot{a} = -\frac{1}{2} \alpha_1 a + \frac{F_1}{2\omega_1} \sin \psi_1 \\ a\dot{\psi}_1 = a\sigma_1 - \frac{3}{8\omega_1} \xi_1 a^3 + \frac{F_1}{2\omega_1} \cos \psi_1 \end{cases} \quad (41)$$

$$\begin{cases} \dot{b} = -\frac{1}{2} \alpha_2 b + \frac{F_2}{2\omega_2} \sin \psi_2 \\ b\dot{\psi}_2 = b\sigma_2 - \frac{3}{8\omega_2} \eta_2 b^3 + \frac{F_2}{2\omega_2} \sin \psi_2 \end{cases} \quad (42)$$

When the system is in steady response,  $\dot{a} = \dot{b} = 0$ , and  $\dot{\psi}_1 = \dot{\psi}_2 = 0$ , combining Eqs. (41) and (42) to eliminate  $\psi_1$  and  $\psi_2$ . The primary resonance amplitude–frequency equation of the system can be obtained as

$$\begin{cases} \frac{9}{16} \xi_1^2 a^4 - 3\omega_1 \xi_1 a^2 \sigma_1 + \omega_1^2 (\alpha_1^2 + 4\sigma_1^2) - \frac{F_1^2}{a^2} = 0 \\ \frac{9}{16} \eta_2^2 b^4 - 3\omega_2 \eta_2 b^2 \sigma_2 + \omega_2^2 (\alpha_2^2 + 4\sigma_2^2) - \frac{F_2^2}{b^2} = 0 \end{cases} \quad (43)$$

### 4 Numerical and analysis

The actual parameters of a 1780 rolling mill are used in numerical simulation. The structure parameters and emulsion parameters of the rolling mill are shown in Table 1, and the dynamic rolling force parameters are shown in Table 2.

#### 4.1 Time-domain characteristics

Figure 4 shows the time-domain curve, phase diagram and Poincaré section of the roll in the vertical direction. It can be seen that the vertical displacement quickly stabilizes, and the amplitude of the vertical displacement fluctuates

stably. The phase diagram is closed, and the Poincaré section is a point, which indicates that the system is a single period motion at this time.

Figure 5 shows the time-domain curve, phase diagram and Poincaré section of the roll in the horizontal direction. It can be seen that the horizontal displacement response quickly stabilizes, but the amplitude fluctuates within a small range ( $10^{-17}$  m). The phase diagram is a closed curve, and the Poincaré section is a point, which indicates that the system is also a single period motion.

Figure 6a shows a three-dimensional view of the change in the film thickness with time and the dimensionless deformation area at the same time. It can be seen that the film thickness gradually decreases and reaches a minimum value at the exit position during the rolling process. Figure 6b shows the time-domain curve at the location of the boundary between the entrance area and the deformation area ( $X = 0$ ). The initial film thickness fluctuates steadily around a certain value that is determined by the rolling process parameters and the emulsion parameters together; thus, the effect of the lubricant film on the quality of the strip can be reduced by changing the process parameters or using different emulsions.

Figure 7 shows the time-domain response of roll’s horizontal displacement, vertical displacement and film thickness when the frequency of the external disturbance force is equal to the natural frequency of the system. It can be seen that the vibration displacement of the roll is larger than those in Figs. 4a, 5a and 6b, which will cause periodic chatter mark and reduce the quality of the product. Therefore, reasonable parameters should be selected to prevent the system from entering a bad state.

#### 4.2 Amplitude–frequency characteristics

The influence of the contact ratio between the interface, the different parameters in the nonlinear rolling force and the change in the amplitude of the external excitation on the amplitude–frequency characteristics of the system was studied based on the equations already obtained.

**Table 1** Structure parameters of 1780 rolling mill

<i>m</i> /kg	<i>y</i> <sub>0</sub> /mm	<i>y</i> <sub>1</sub> /mm	<i>R</i> /mm	<i>v</i> <sub>R</sub> /(m s <sup>-1</sup> )	<i>σ</i> /MPa	<i>k</i> <sub>1</sub> /(N m <sup>-1</sup> )	<i>k</i> <sub>2</sub> /(N m <sup>-1</sup> )	<i>c</i> <sub>1</sub> /(N s m <sup>-1</sup> )	<i>c</i> <sub>2</sub> /(N s m <sup>-1</sup> )	<i>μ</i> <sub>0</sub> /(Pa s)	<i>γ</i> /Pa <sup>-1</sup>
$1.44 \times 10^5$	14.1	8.2	420	4	150.6	$2.01 \times 10^{10}$	$1.8 \times 10^{11}$	$2 \times 10^6$	$8.65 \times 10^5$	0.42	$2 \times 10^{-8}$

**Table 2** Dynamic rolling force parameters of 1780 rolling mill

<i>a</i> <sub>1</sub>	<i>a</i> <sub>2</sub>	<i>a</i> <sub>3</sub>	<i>a</i> <sub>4</sub>	<i>a</i> <sub>5</sub>	<i>a</i> <sub>6</sub>	<i>a</i> <sub>7</sub>	<i>b</i> <sub>1</sub>	<i>b</i> <sub>2</sub>	<i>b</i> <sub>3</sub>	<i>b</i> <sub>4</sub>	<i>b</i> <sub>5</sub>	<i>b</i> <sub>6</sub>	<i>b</i> <sub>7</sub>
0	$3.14 \times 10^{10}$	$-2.52 \times 10^7$	$4.75 \times 10^8$	-29.29	0	$4.98 \times 10^{15}$	0	$3.48 \times 10^9$	$-8.04 \times 10^6$	$1.51 \times 10^5$	0.91	0	$1.87 \times 10^{14}$

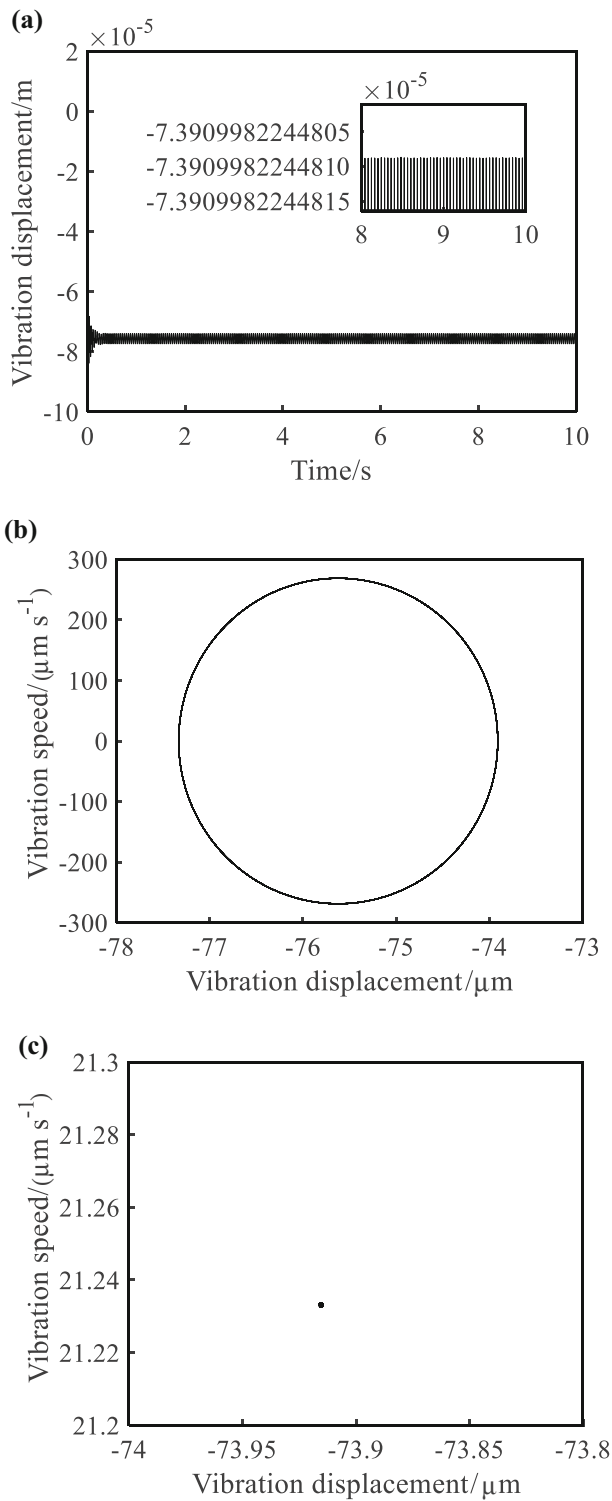


**Fig. 4** Vertical time-domain curve (a), phase diagram (b) and Poincaré section (c)

Figure 8 shows the amplitude–frequency curves for different contact ratios. It can be seen that as  $\lambda$  increases, the proportion of fluid friction decreases, the primary

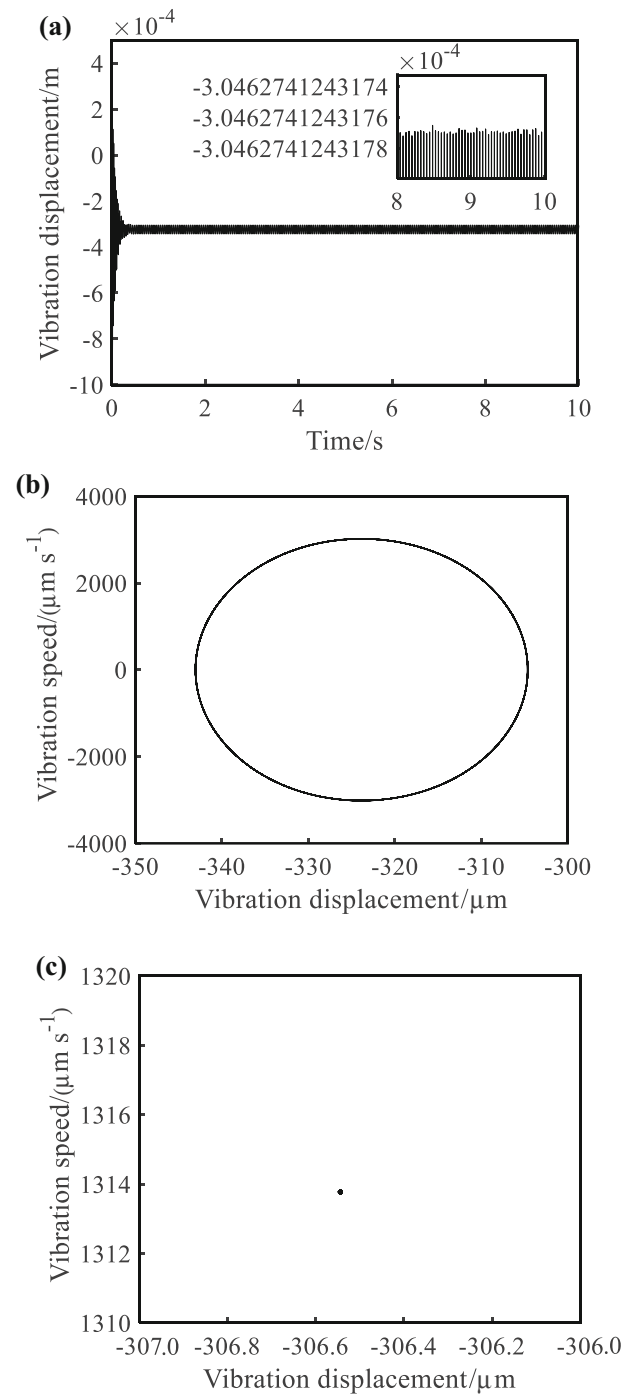


**Fig. 5** Horizontal time-domain curve (a), phase diagram (b) and Poincaré section (c)

resonance amplitude value decreases and the jumping phenomenon is more obvious. Therefore, the appropriate rolling process parameters and emulsion can reduce the primary resonance amplitude value of the system and the jumping phenomenon.



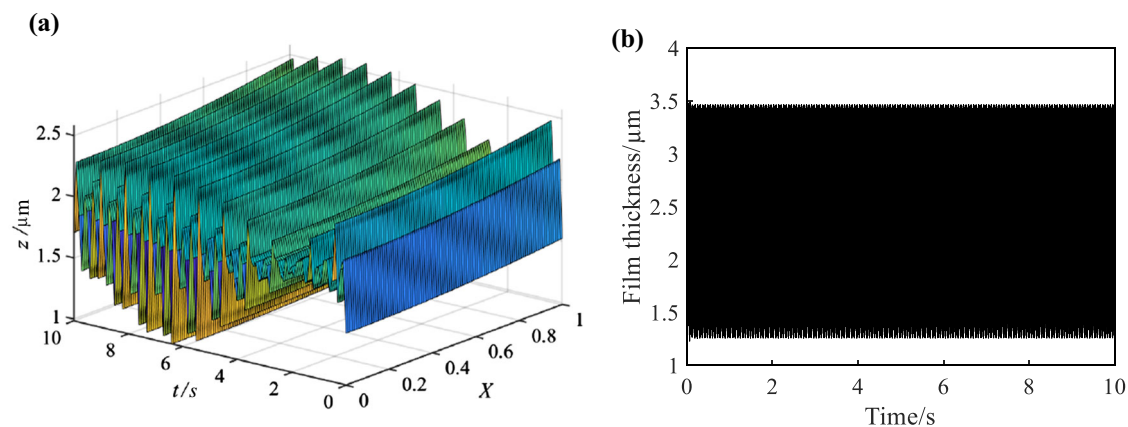


**Fig. 6** Lubricant film thickness change. **a** Film thickness in deformation area; **b** film thickness curve

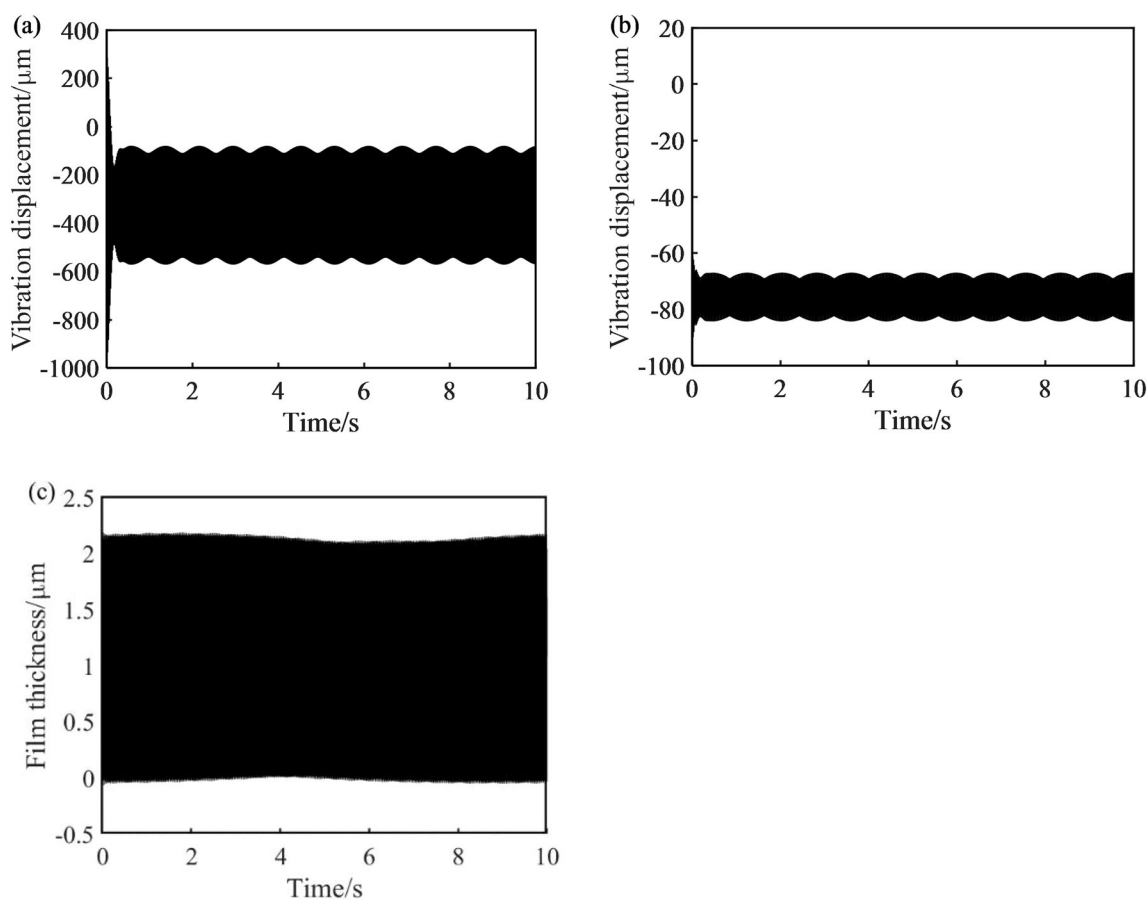


**Fig. 7** Time-domain curve under instability. **a** Horizontal displacement; **b** vertical displacement; **c** film thickness

Figures 9–13 show the primary resonance amplitude–frequency characteristics of the rolling mill with different vertical direction parameters.

Figures 9 and 10 show the amplitude–frequency characteristic curves in the vertical direction under the changes of parameter  $b_2$  and  $b_4$ , respectively. The primary

resonance amplitude can be seen in the picture will decrease and the occurrence of the jumping phenomenon will be curbed as parameters  $b_2$  and  $b_4$  increase.

Figure 11 shows the amplitude–frequency diagram of primary resonance when the coefficients of different nonlinear stiffness terms change. It can be seen that the

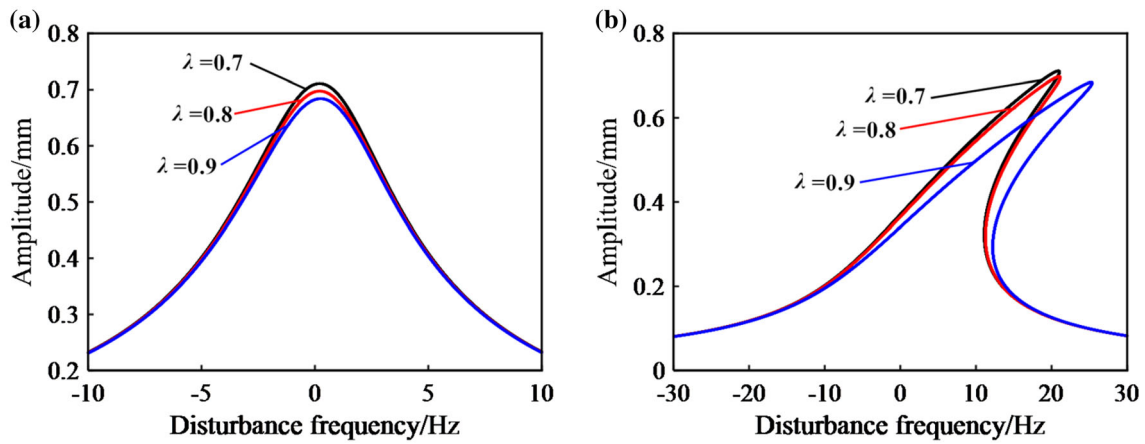


Fig. 8 Primary resonance at different contact ratios. **a**  $b_7 = 1.87 \times 10^{14}$ ; **b**  $b_7 = 1.87 \times 10^{16}$

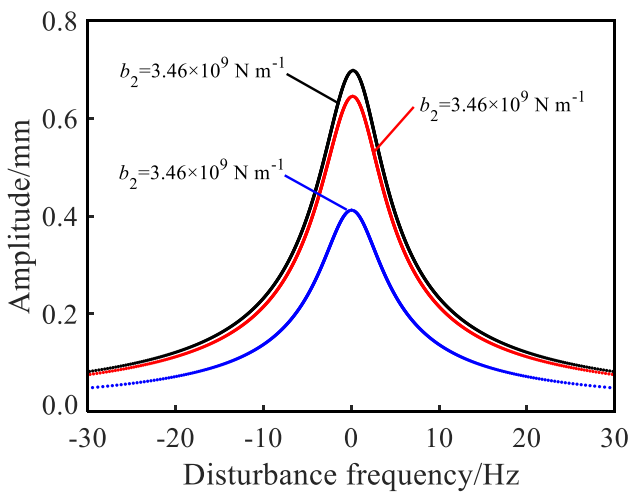


Fig. 9 Primary resonance amplitude–frequency curve of different  $b_2$  in vertical direction

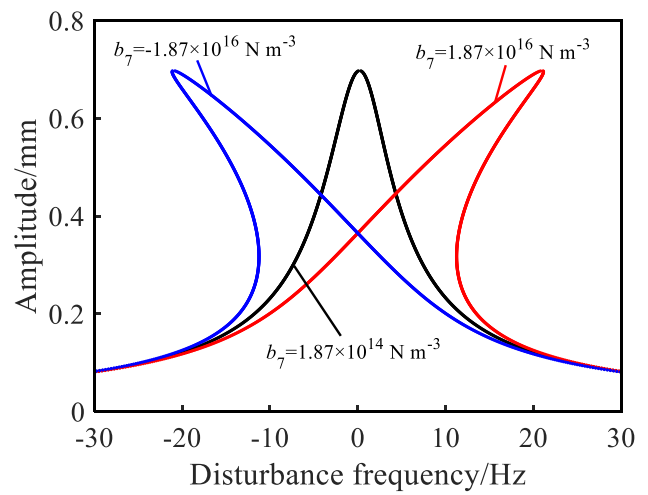


Fig. 11 Primary resonance amplitude–frequency curve of different  $b_7$  in vertical direction

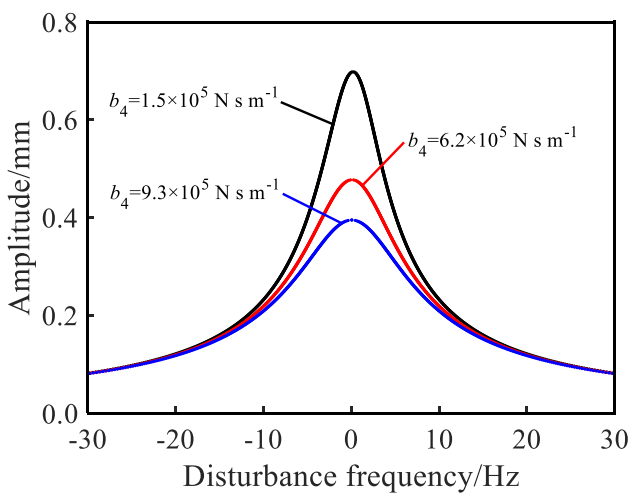


Fig. 10 Primary resonance amplitude–frequency curve of different  $b_4$  in vertical direction

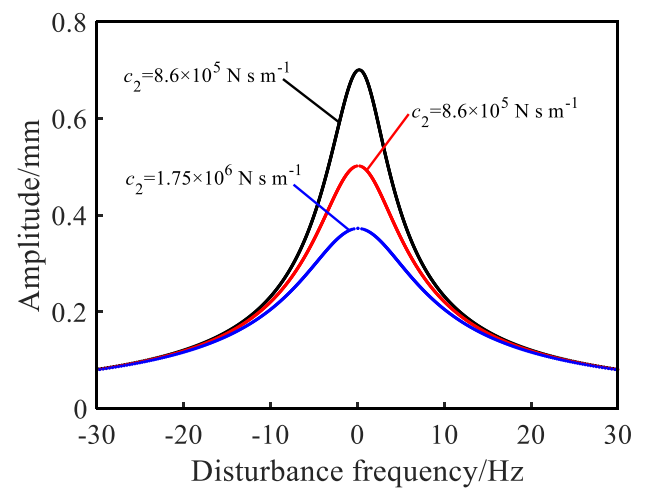
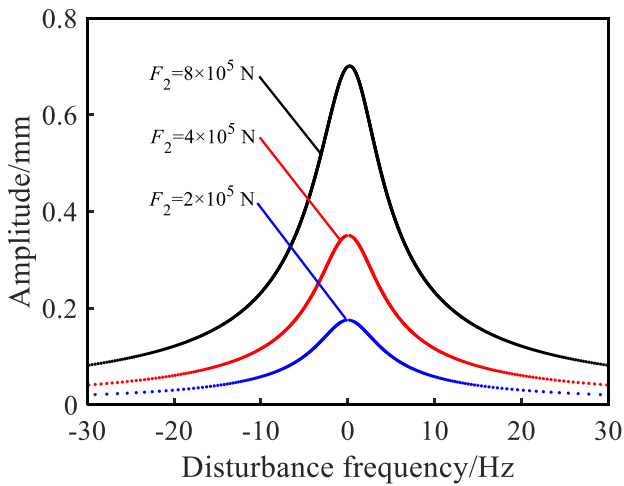
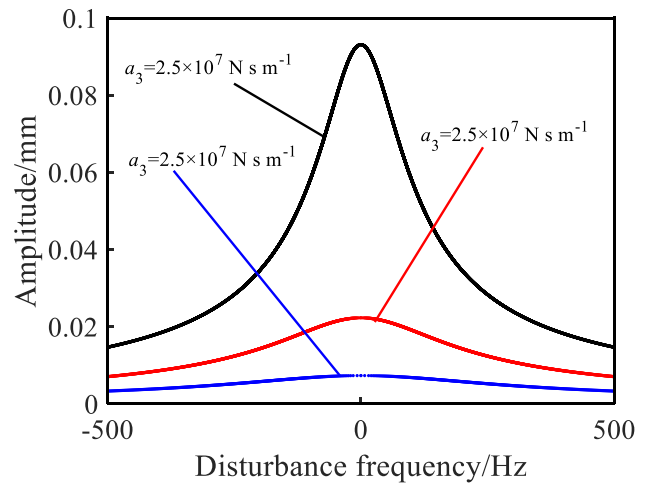


Fig. 12 Primary resonance amplitude–frequency curve of different damping  $c_2$  in vertical direction



**Fig. 13** Primary resonance amplitude–frequency curve of different external disturbances  $F_2$  in vertical direction



**Fig. 16** Primary resonance amplitude–frequency curve of different  $a_3$  in horizontal direction

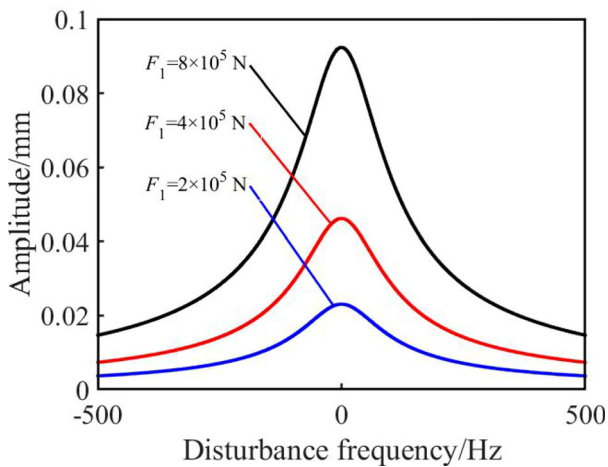


**Fig. 14** Primary resonance amplitude–frequency curve of different external disturbances  $F_1$  in horizontal direction

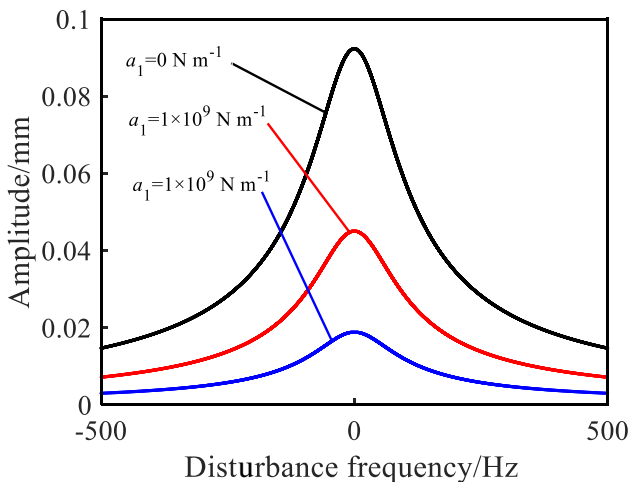


**Fig. 15** Primary resonance amplitude–frequency curve of different  $a_1$  in horizontal direction

parameter  $b_7$  is related to the jumping phenomenon of the system.

Figure 12 shows the primary resonance amplitude–frequency of different damping in the vertical direction. It can be seen that the amplitude of the primary resonance of the rolling mill will decrease as damping  $c_2$  increases.

Figure 13 shows a primary resonance amplitude–frequency diagram with different external disturbances  $F_2$  in vertical direction. An increase in the amplitude of the external disturbance force  $F_2$  causes an increase in the maximum amplitude of the primary resonance in the vertical direction in Fig. 13.

Figures 14–16 show the amplitude–frequency characteristic curves of the rolling mill under different horizontal direction parameters. It can be seen that there is no jumping phenomenon in these Figs. 14–16. The change of the parameters only affects the magnitude of the primary resonance amplitude value.

### 5 Conclusions

1. The dynamic expression of the lubricant film is derived when the work roll vibrates. A dynamic rolling force model under mixed lubrication friction conditions is established, and a vertical-horizontal coupled vibration dynamic model of the rolling system is established.
2. The amplitude–frequency characteristics of the system of different parameters are obtained. In the  $y$  (vertical) direction, the nonlinear term parameter  $b_7$  will cause the system to jump, increasing camping term  $c_2$  can effectively reduce the amplitude of the primary resonance and increasing the magnitude of external disturbance  $F_2$  can increase the primary resonance amplitude value. In the  $x$  (horizontal) direction,

parameters only affect the primary resonance amplitude value, but will not affect the system's jumping phenomenon. Therefore, the appropriate system parameters are selected to reduce the rolling mill vibration.

3. The interface contact ratio affects the primary resonance amplitude–frequency characteristic curve of the system. The larger the proportion of hydrodynamic lubrication, the larger the primary resonance amplitude value, and the stronger the jumping phenomenon. Therefore, the primary resonance amplitude value of the system can be reduced by selecting appropriate rolling process parameters or emulsions.

**Acknowledgements** This research is supported by the National Natural Science Foundation of China (Grant Nos. 61973262 and 51405068) and the Natural Science Foundation of Hebei Province of China (Grant No. E2019203146).

## References

- [1] Z.Y. Gao, Y. Zang, L.Q. Zeng, *Journal of Mechanical Engineering* 51 (2015) No. 16, 87–105.
- [2] Matsuo Ataka, *ISIJ Int.* 55 (2015) 89–102.
- [3] J.M. Li, X.F. Chen, Z.J. He, *J. Sound Vibr.* 332 (2013) 5999–6015.
- [4] J.L. Huang, Y. Zang, Z.Y. Gao, L.Q. Zeng, *J. Vibroeng.* 19 (2017) 4840–4853.
- [5] Y.A. Amer, A.T. EL-Sayed, F.T. El-Bahrawy, *J. Mech. Sci. Technol.* 29 (2015) 1581–1589.
- [6] P.M. Shi, J.Z. Li, J.S. Jiang, B. Liu, D.Y. Han, *J. Iron Steel Res. Int.* 20 (2013) 7–12.
- [7] J.L. Sun, Y. Peng, H.M. Liu, *Chin. J. Mech. Eng.* 26 (2013) 144–150.
- [8] X.X. Wang, X.Q. Yan, *Math. Probl. Eng.* 2019 (2019) 5868740.
- [9] H.R. Liu, D.X. Hou, P.M. Shi, F. Liu, *Journal of Mechanical engineering* 47 (2011) No. 13, 65–71.
- [10] S. Liu, Y.T. Shi, Y.P. Zhang, M. Zong, *J. Vibroeng.* 19 (2017) 2188–2201.
- [11] X. Lu, J. Sun, G.T. Li, Z.H. Wang, D.H. Zhang, *Shock Vib.* 2019 (2019) 4358631.
- [12] L.Q. Zeng, Y. Zang, Z.Y. Gao, *Shock Vib.* 2016 (2016) 2347386.
- [13] W.G. Li, C. Liu, N. Feng, X. Chen, X.H. Liu, *J. Iron Steel Res. Int.* 23 (2016) 1268–1276.
- [14] D.X. Hou, R.R. Peng, H.R. Liu, *Shock Vib.* 2014 (2014) 543793.
- [15] L.Q. Zeng, Y. Zang, Z.Y. Gao, *J. Vibroeng. Acoust.* 139 (2017) 061015.
- [16] X.C. Liu, Y. Zang, Z.Y. Gao, L.Q. Zeng, *J. Vibroeng.* 19 (2017) 1569–1584.
- [17] Q.Y. Wang, Z. Zhang, H.Q. Chen, C.S. Feng, *Int. J. Surf. Sci. Eng.* 9 (2015) 343–358.
- [18] N. Patir, H.S. Cheng, *J. Lubr. Technol. ASME* 100 (1978) 12–17.
- [19] J.A. Schey, *Lubr. Eng.* 39 (1983) 376–382.
- [20] I.S. Yun, W.R.D. Wilson, K.F. Ehmann, *J. Manuf. Sci. Eng.* 120 (1998) 330–336.
- [21] P.H. Hu, K.F. Ehmann, *Int. J. Mach. Tools Manuf.* 40 (2000) 1–19.